Optical absorption in semiconductor quantum dots: A tight-binding approach

Lavanya M. Ramaniah
Theoretical Physics Division, Bhabha Atomic Research Centre, Bombay 400 085, India

Selvakumar V. Nair
Laser Programme, Centre for Advanced Technology, Indore 452 013, India
(Received 1 April 1992; revised manuscript received 6 August 1992)

We present a tight-binding calculation of the interband optical transitions in semiconductor quantum dots (QD's). The calculated optical-absorption spectra are in good agreement with the existing experimental spectra of CdS and CdSe QD's. We establish a correspondence between the tight-binding (TB) energy levels and those calculated using the spherical multiband effective-mass approximation (EMA). Consequently, the comparatively stringent selection rules of the latter are applicable to a large extent. Thus we formulate a convenient and quantitatively accurate description of the optical absorption in QD's in terms of the TB energy levels and multiband EMA quantum numbers.

I. INTRODUCTION

Semiconductor quantum dots (QD's) have been attracting considerable attention in recent years. This interest has mainly focused on understanding various quantum size effects[1] in these nanocrystallites, which are small compared to the bulk exciton Bohr radius. From the applied physics point of view, the possibility of obtaining novel and tailorable optical properties,[2] together with their smallness of size, makes QD's promising candidates for quantum semiconductor devices. A large number of experiments probing the electronic structure and the optical spectra of quantum dots have been performed, particularly on CdS and CdSe quantum dots.[3–15] Recent experiments[4,5] on well-characterized samples have resolved a number of features showing size-quantized energy-level structure in the absorption and photoluminescence excitation (PLE) spectra.

For interpreting the optical-absorption spectra, the single-band effective-mass approximation[16] (EMA) is widely used mainly due to its simplicity. As both intervalence-band mixing and deviation from quadratic dispersion are neglected by single-band EMA, no rigorous quantitative comparison between this theory and experiment has been possible. Although band mixing can be included within the EMA by multiband calculations,[17–20] one has to go beyond the EMA to get quantitatively accurate energy levels, especially in smaller QD's. In fact, recent tight-binding (TB) calculations[21–23] give energy levels in good agreement with the measured size dependence of the absorption edge and of the valence-band edge.

In this paper, we present a tight-binding calculation of the interband optical transitions of quantum dots. Specifically, we consider spherical QD's of cubic CdS and CdSe, with sizes ranging from 10 to 60 Å in diameter. The calculated optical-absorption spectra are in good quantitative agreement with the best existing experimental spectra. Further, we find that some of the peaks observed in the absorption, and even in the PLE spectra, are actually made up of more than one transition, which may get resolved in better samples. In view of this, we give detailed numerical results on the transition frequencies and oscillator strengths of CdS and CdSe QD's of various sizes.

One drawback of a tight-binding description of the optical-absorption spectrum is the lack of stringent selection rules, as exist, for example, in the EMA in the spherical band approximation. Hence we seek to establish a correspondence between the TB and multiband EMA energy levels, and find that the selection rules of the latter are applicable to a large extent. Thus, we formulate a description of the optical absorption in QD's, which has the quantitative accuracy of TB theory and the qualitative simplicity of the spherical approximation.

The paper is organized as follows. In Sec. II, we discuss the theoretical method of calculating the interband absorption spectrum. In Sec. III, we present and discuss the selection rules and oscillator strengths for interband transitions, and compare the calculated optical-absorption spectra for CdSe and CdS QD's with the existing experimental spectra. Finally, in Sec. IV we summarize our conclusions.

II. THEORETICAL METHOD

To calculate the optical-absorption spectrum in a quantum dot, one requires the energy levels and the oscillator strengths for transitions between the various energy levels. The oscillator strength for a transition from a level i to a level j is given by

$$f_{ij}=2|\langle i|\boldsymbol{\eta}\cdot\mathbf{p}|j\rangle|^2/(m_0\hbar\omega_{ij}) , \quad (1)$$

where $\boldsymbol{\eta}$ is the photon polarization, $\mathbf{p}$ is the electron momentum operator, and ω_{ij} is the transition frequency. It may be noted that a spherical QD of cubic material is optically isotropic, and the oscillator strength is polarization independent.

TABLE I. The parametrization scheme used for obtaining the EBOM parameters. The parameter values used for CdS and CdSe are given in the right column.

Parametrization scheme	Parameters used	CdS	CdSe
$E_s = E_c^{L_1}$	$E_s =$	4.157	3.344
$E_{ss} = (E_c^{L_1} - E_c^{X_1})/4$	$E_{ss} =$	−0.134	−0.121
$E_{xx} = (E_v^{\Gamma_{15}} - E_v^{X_3})/16$	$E_{xx} =$	0.319	−0.281
$E_p = (2E_v^{X_5} + E_v^{\Gamma_{15}} + E_v^{X_3})/4$	$E_p =$	−2.245	−2.5
$E_{xy} = (-E_p + E_v^{L_3})/4$	$E_{xy} =$	0.286	0.325
$E_{zz} = (E_v^{X_3} + E_v^{\Gamma_{15}} - 2E_v^{X_5})/16$	$E_{zz} =$	−0.0013	−0.0125
$E_{sx} = [(E_{ss} + \hbar^2/2m_e^* a^2)E_g/16]^{1/2}$			

To calculate the energy levels and the eigenfunctions of the QD, we use an empirical tight-binding model, the effective-bond-orbital model[24] (EBOM), in which the structure of the zinc-blende semiconductor is replaced by an effective fcc lattice. Two s-like conduction-band (CB) orbitals together with six p-like valence-band (VB) orbitals make up a basis of eight orbitals per fcc site (including spin). The Hamiltonian matrix elements between these "bond orbitals" are of the Slater-Koster form,[25] with only nearest-neighbor interactions included. These have been described in considerable detail earlier.[22,24,26] The tight-binding parameters may be fixed empirically. We use a parametrization which grossly reproduces, in the bulk limit, the main features of the relevant bands along the symmetry directions of the Brillouin zone with just the seven parameters of the EBOM.[22] The parametrization scheme, as well as the values of the parameters for CdS and CdSe, are given in Table I. The symmetry-point energy values E^{Γ}, E^{X}, etc. for cubic CdS and CdSe were taken from Ref. 27. Spin-orbit interaction is also included.[22,26] As noted earlier,[22] more accurate energy levels of the quantum dot are obtained with this parametrization scheme, which reproduces the band dispersion throughout the Brillouin zone reasonably accurately, than with a parametrization scheme based on the band-edge dispersion only.[24] The bulk band structures for CdS and CdSe, obtained by using the parameters given in Table I, compare well with the band structures calculated in Ref. 27.

The Hamiltonian of the spherical QD is next constructed by making extensive use of point-group symmetry.[22,26] For spherical quantum dots with fcc structure, the symmetry group is O_h, and the eigenfunctions must belong to the irreducible representations of the O_h double group, viz., $\Gamma_6^{\pm}$, $\Gamma_7^{\pm}$, $\Gamma_8^{\pm}$ having degeneracy 2, 2, and 4, respectively. The QD Hamiltonian is constructed in each symmetry-selected subspace, and is diagonalized, and the eigenvalues and eigenfunctions are obtained. These eigenfunctions are now known linear combinations of the bond orbitals on each fcc site of the crystallite.

The dipole transition matrix elements between the eigenfunctions of the QD can be obtained in terms of the matrix elements of the dipole operator between the bond orbitals. The latter are given by

$$P^{\beta}_{\alpha\alpha'}(\mathbf{R}_i - \mathbf{R}_j) = -i\hbar\sqrt{2/m_0}\int d^3r\, \varphi_{\alpha}(\mathbf{r}-\mathbf{R}_i) \times \partial/\partial\beta\, \varphi_{\alpha'}(\mathbf{r}-\mathbf{R}_j)\ , \quad (2)$$

where α and α' refer to the s, p_x, p_y, and p_z bond orbitals, $\beta = x$, y, and z is the polarization of the incident photon, and $\varphi_{\alpha}(\mathbf{r}-\mathbf{R}_i)$ is the αth bond orbital centered at lattice position $\mathbf{R}_i$.

In the size range considered by us, for CdS and CdSe, there is negligible mixing of s and p orbitals in the eigenfunctions of the lowest few levels of the QD. Hence the interband transition matrix elements involve dipole matrix elements between s and p orbitals only. Further, we assume that only the on-site momentum matrix elements are nonzero, which is equivalent to assuming a flat $\mathbf{k}$ dependence for the bulk momentum matrix elements. The on-site momentum matrix elements between the s and p orbitals, $P^{\beta}_{s\gamma}(0)$, can be written, using cubic symmetry, as

$$P^{\beta}_{s\gamma}(0) = i\delta_{\gamma\beta}Q_{sp}\ ,$$

where γ refers to the p_x, p_y, and p_z orbitals, and

$$Q_{sp} = -\hbar\sqrt{2/m_0}\int d^3r\, \varphi_s(\mathbf{r})\partial/\partial\beta\, \varphi_{\beta}(\mathbf{r})\ . \quad (3)$$

It can be seen that Q_{sp} is equal to the square root of the Kane momentum matrix element E_K, which may be obtained empirically from[28]

$$(1/m_e^* - 1) = 2E_K/3E_g + E_K/3(E_g + \Delta)\ ,$$

where m_e^* is the conduction-band effective mass in units of the free-electron mass, E_g is the fundamental band gap, and Δ is the spin-orbit splitting. The values of E_K calculated for CdS and CdSe are given in Table II.

TABLE II. The values of various material parameters for CdS and CdSe used in the calculation.

	CdS	CdSe
Spin-orbit splitting (Δ) (eV)	0.06	0.424
Kane momentum matrix element (E_K) (eV)	15.47	16.37
Lattice constant (a) (Å)	5.82	6.01
Conduction-band mass (m_e^*)	0.14	0.11
Band gap (E_g)		
(a) cubic form	2.55 (0 K)	1.9 (0 K)
(b) hexagonal form	2.58 (0 K)	1.84 (0 K)
	2.45 (300 K)	1.74 (300 K)
Dielectric constant (ϵ)	6	7

III. RESULTS AND DISCUSSION

A. Selection rules and oscillator strengths

In the EBOM calculation, the group-theoretic selection rules for dipole transitions indicate only that all interband transitions between a VB level and a CB level with opposite parity are allowed, except the $\Gamma_6^{\pm}$-to-$\Gamma_6^{\mp}$ and the $\Gamma_7^{\pm}$-to-$\Gamma_7^{\mp}$ transitions. On the other hand, the selection rules in the EMA, in the spherical-band approximation, are more stringent viz., $\Delta L=0$, where L is the envelope-function angular momentum. Hence a more convenient description of the interband transitions may be obtained by establishing a correspondence between the EBOM and EMA energy levels. This is, in fact, possible, because both the energy level structure and the wave functions in the EBOM and the multiband EMA are qualitatively similar,[22] even though, as mentioned earlier, the electron-hole confinement energies are incorrectly estimated in the EMA. Thus, the EMA selection rules apply to a large extent to the EBOM also, for transitions between corresponding energy levels. This procedure, of describing the interband transitions predicted by the EBOM in terms of the EMA envelope function labels, will be illustrated as we specifically consider the cases of CdS and CdSe QD's. It may be noted that the EMA wave functions are generally only weakly affected by the cubic perturbation caused by the underlying lattice in the EBOM and are absent in the spherical-band EMA. However, if two EMA levels are close by, they may get mixed by the cubic perturbation, leading to considerable modification of the EMA-derived selection rules.

The CB levels are qualitatively well described by the single-band EMA, while the multiband EMA is required to describe the VB. For a semiconductor like CdS with spin-orbit splitting small compared to the confinement energies, a three-band model (without spin) is appropriate for the VB, while for materials with large spin-orbit splitting, a four-band Luttinger model for the Γ_8 ($J=\frac{3}{2}$) band and a single-band model for the Γ_7 ($J=\frac{1}{2}$) band may be used. In CdSe QD's of the sizes considered by us, the situation is somewhat intermediate to these two extremes.

At this point, we digress to describe the TB and EMA notations which we use for the energy levels. In the TB scheme, the nth level of Γ_ν symmetry and $\pm$ parity is denoted by $n\Gamma_\nu^{\pm}$. In the multiband EMA, levels are characterized by the quantum numbers n, F, and $\pm$, where n is the radial quantum number and F ($=J+L$) is the total angular momentum. Here, J is the angular momentum of the Bloch function and L is that of the envelope function. Alternatively, the multiband EMA levels may also be denoted by the L values which make up a given F value. We use the latter notation, as it is more transparent in determining the dipole selection rules. Following Ref. 18, the angular momenta of the envelope functions are denoted by capital letters S, P, D, F, etc, in the multiband EMA and by small letters s, p, d, f, etc., in the single-band EMA (i.e., for the CB, and the splitoff band in the four-band model). However, this notation is ambiguous for the four-band model, as the same combination of L values corresponds to two different F values, as, e.g., S and D envelope functions mix to give both $F=\frac{3}{2}$ and $\frac{5}{2}$ energy levels. Hence in the four-band model, we also indicate the F value as a subscript.

Tables III and IV give the electron-hole confinement energies and oscillator strengths for the first few transitions in CdS and CdSe QD's, respectively. All of the transitions listed in the tables involve the lowest three CB levels, viz., the $1\Gamma_6^+$ and the $1\Gamma_7^-$ and $1\Gamma_8^-$, which correspond to the $l=0$, $n=1$ ($1s$) and $l=1$, $n=1$ ($1p$) EMA levels,[22] respectively. The interband transition between the nth VB energy level of $\Gamma_\nu^{\pm}$ symmetry and the mth CB level of $\Gamma_\mu^{\mp}$ symmetry is denoted by $n\Gamma_\nu^{\pm}-m\Gamma_\mu^{\mp}$. The confinement energies quoted are the confinement kinetic energies, and do not include Coulomb interaction. The interband transition energy would be $E_{\text{trans}}=E_g^{\text{bulk}}+E_{\text{conf}}+E_{\text{Coul}}$.

In Fig. 1, the qualitative structure of the VB and CB levels near the band edge for CdS, given by the EBOM and the three-band EMA, are compared. Also shown are the allowed interband transitions. The splittings of the EMA levels into EBOM levels are due to the spin-orbit interaction as well as the cubic perturbation. The transitions listed in Table III mainly correspond to the four EMA transitions shown in Fig. 1, viz., between the $1P^+$, $1(P+F)^+$, $1(S+D)^-$, and $2(S+D)^-$ VB levels and the $1s^+$ and $1p^-$ CB levels. An interesting exception is the $1\Gamma_7^+$ to $1\Gamma_8^-$ transition, which appears for $R=11.8$ and 14.3 Å. This can be understood as follows. The $1\Gamma_7^+$ VB level corresponds to the $1F^+$ level in the EMA but acquires a small P component due to mixing, with the close-by $1(P+F)^+$ level, induced by the cubic crystal field. This mixing is strong enough to show up in the oscillator strength only for a small size range for which the levels mentioned are close enough. The splitting of the topmost VB level, $1(S+D)^-$ in the EMA, into $1\Gamma_8^-$ and $1\Gamma_7^-$ in EBOM, is mainly due to the spin-orbit interac-

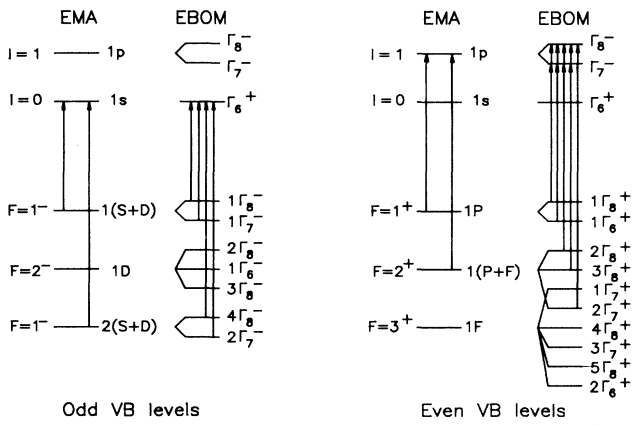

FIG. 1. Correspondence between the qualitative level structure of the near-band-edge energy levels obtained using the EBOM and the EMA, for CdS QD's. In the EMA, a three-band model for the valence band (VB) and a single-band model for the conduction band (CB) have been used. The interband transitions, allowed according to the EMA selection rules, are also indicated.

TABLE III. The electron-hole-pair confinement kinetic energies (E) and the oscillator strengths (f) for the first few interband transitions in CdS QD's, for various sizes, obtained using a tight-binding calculation (TB). For each transition $n\Gamma_{\mu}^{\pm}$-to-$m\Gamma_{\mu}^{\mp}$, the corresponding EMA notation is indicated. The energies are in eV, and the sizes in Å. We note that the Coulomb energy and the bulk band gap are to be added to the confinement energy E to get the transition frequency. The EMA notation corresponds to a three-band model for the valence band (VB) and to a single-band model for the conduction band (CB).

Transitions		Radius (Å)	8.7		11.8		14.3		17.5		20.0		23.2	
TB notation	EMA notation		E	f	E	f	E	f	E	f	E	f	E	f
$1\Gamma_8^-$-$1\Gamma_6^+$	$1(S+D)$-$1s$		1.43	3.34	1.01	3.72	0.8	4.11	0.6	4.14	0.5	4.02	0.4	4.13
$1\Gamma_7^-$-$1\Gamma_6^+$	$1(S+D)$-$1s$		1.48	1.59	1.06	1.76	0.85	1.91	0.65	1.75	0.55	1.71	0.45	1.73
$4\Gamma_8^-$-$1\Gamma_6^+$	$2(S+D)$-$1s$		1.99	0.93	1.36	0.83	1.07	0.9	0.8	0.97	0.65	0.9	0.52	0.79
$2\Gamma_7^-$-$1\Gamma_6^+$	$2(S+D)$-$1s$		2.02	0.53	1.39	0.52	1.09	0.58	0.82	0.7	0.67	0.75	0.54	0.87
$1\Gamma_8^+$-$1\Gamma_7^-$	$1P$-$1p$		1.99	0.67	1.45	0.8	1.17	0.94	0.91	1.09	0.75	1.34	0.62	1.48
$1\Gamma_8^+$-$1\Gamma_8^-$	$1P$-$1p$		1.99	2.73	1.45	2.9	1.17	2.88	0.91	2.93	0.75	2.76	0.62	2.28
$1\Gamma_6^+$-$1\Gamma_7^-$	$1P$-$1p$		2.02	1.15	1.48	1.25	1.2	1.35	0.94	1.42	0.78	1.52	0.65	1.41
$1\Gamma_6^+$-$1\Gamma_8^-$	$1P$-$1p$		2.02	0.54	1.48	0.6	1.2	0.62	0.94	0.67	0.78	0.71	0.65	0.69
$2\Gamma_8^+$-$1\Gamma_8^-$	$1(P+F)$-$1p$		2.31	1.04	1.68	1.31	1.35	1.26	1.05	1.38	0.87	1.49	0.71	1.53
$2\Gamma_8^+$-$1\Gamma_7^-$	$1(P+F)$-$1p$		2.31	0.26	1.68	0.29	1.35	0.34	1.05	0.36	0.87	0.33	0.71	0.32
$2\Gamma_7^+$-$1\Gamma_8^-$	$1(P+F)$-$1p$		2.44	0.97	1.81	0.53	1.45	0.73	1.13	1.1	0.95	1.13	0.77	1.12
$3\Gamma_8^+$-$1\Gamma_7^-$	$1(P+F)$-$1p$		2.45	0.95	1.81	0.86	1.45	0.92	1.13	0.84	0.95	0.65	0.77	0.56
$3\Gamma_8^+$-$1\Gamma_8^-$	$1(P+F)$-$1p$		2.45	0.86	1.81	0.67	1.45	0.46	1.13	0.27	0.95	0.24	0.77	0.23
$1\Gamma_7^+$-$1\Gamma_8^-$	$1F$-$1p$		2.42	0.09	1.79	0.55	1.44	0.3	1.1	0.04	0.91	<0.01	0.74	0.02

TABLE IV. Same as in Table III, but for CdSe QD's. The EMA notation corresponds to a four-band model for the $J=\frac{3}{2}$ VB, and to a single-band model for the CB and the split-off VB. The blanks for the $1d$-$1s$ transition indicate that the oscillator strength is almost zero.

Transitions		Radius (Å)	8.9		12.2		14.8		18.1		20.7		24.0		26.9	
TB notation	EMA notation		E	f	E	f	E	f	E	f	E	f	E	f	E	f
$1\Gamma_8^-$-$1\Gamma_6^+$	$1(S+D)_{3/2}$-$1s$		1.45	4.07	1.03	4.58	0.82	5.08	0.63	5.1	0.52	4.85	0.42	4.85	0.35	4.66
$1\Gamma_7^-$-$1\Gamma_6^+$	$1s$-$1s$		1.79	1.46	1.37	1.41	1.14	1.16	0.92	0.51	0.78	0.01	0.63	0.03	0.53	<0.01
$3\Gamma_8^-$-$1\Gamma_6^+$	$2(S+D)_{3/2}$-$1s$		1.99	0.66	1.37	0.94	1.08	1.22	0.8	1.69	0.65	1.96	0.52	2.33	0.44	2.45
$1\Gamma_8^+$-$1\Gamma_7^-$	$1(P+F)_{3/2}$-$1p$		2.0	1.26	1.46	1.67	1.18	2.10	0.92	2.58	0.77	2.87	0.63	2.76	0.54	2.66
$1\Gamma_8^+$-$1\Gamma_8^-$	$1(P+F)_{3/2}$-$1p$		2.01	2.73	1.47	2.77	1.19	2.56	0.93	2.23	0.78	2.3	0.64	2.21	0.54	2.13
$4\Gamma_8^-$-$1\Gamma_6^+$	$1d$-$1s$		2.18	0.52	1.57	0.19	1.27	<0.01	0.98	0.02						
$1\Gamma_6^+$-$1\Gamma_7^-$	$1p$-$1p$		2.21	1.44	1.68	1.58	1.4	1.76	1.13	2.0	0.98	2.07	0.83	1.11	0.71	0.08
$1\Gamma_6^+$-$1\Gamma_8^-$	$1p$-$1p$		2.22	0.45	1.69	0.46	1.41	0.45	1.14	0.36	0.98	0.27	0.84	0.10	0.71	<0.01
$2\Gamma_7^-$-$1\Gamma_6^+$	$2s$-$1s$		2.28	0.74	1.62	0.75	1.29	0.5	1.01	0.74	0.85	0.81	0.72	0.61	0.63	0.08
$2\Gamma_8^+$-$1\Gamma_8^-$	$1(P+F)_{5/2}$-$1p$		2.39	1.58	1.74	1.82	1.41	1.83	1.1	1.88	0.92	1.92	0.75	1.89	0.63	1.63
$1\Gamma_7^+$-$1\Gamma_8^-$	$1(P+F)_{5/2}$-$1p$		2.48	0.84	1.85	1.05	1.49	1.11	1.15	0.9	0.95	0.71	0.78	0.62	0.66	0.67
$3\Gamma_7^-$-$1\Gamma_6^+$	$1(D+G)_{7/2}$-$1s$		2.56	0.01	1.78	0.45	1.43	0.97	1.14	0.99	0.93	0.04	0.76	<0.01	0.64	0.35

tion, which leads to a 60 meV splitting in the bulk. It is interesting to note that for the whole size range considered, this splitting in the QD is 48–50 meV, which is close to the first-order perturbation-theoretic estimate[23] of 48 meV within the multiband EMA. The $1P^+$ VB level splits into $1\Gamma_8^+$ and $1\Gamma_6^+$, with a separation of 29–31 meV, again in close agreement with the first-order perturbation-theoretic estimate of 30 meV.

The order and the oscillator strengths of the first few transitions in CdSe, shown in Table IV, differ from those of CdS mainly because the spin-orbit splitting in CdSe is much larger. Much of Table IV can be understood within the framework of the four-band Luttinger model for the $J=\frac{3}{2}$ bands, and the single-band model for the splitoff ($J=\frac{1}{2}$) band.[18] The qualitative level structure and transitions obtained in the four-band model are compared with those obtained in the EBOM in Fig. 2.

We consider first the transitions involving the odd-parity VB levels. In addition to the two transitions from the $J=\frac{3}{2}$ bands shown in Fig. 2, Table IV also lists transitions from the splitoff band. The first level corresponding to the splitoff band is of Γ_7^- symmetry ($1s^-$ in the EMA) and for small sizes it lies above the first Γ_7^- level arising from the $J=\frac{3}{2}$ bands. As the crystallite size increases, the confinement energies decrease and the Γ_7^- levels corresponding to the $J=\frac{3}{2}$ bands cross the splitoff Γ_7^- levels. For the smallest size considered by us, the $1\Gamma_7^-$ and the $2\Gamma_7^-$ levels involve the splitoff band. For the largest size they arise from the $J=\frac{3}{2}$ band and correspond to the $F=7/2^-$ EMA level (see Fig. 2), which does not have an S component. Thus the $1\Gamma_7^-$-to-$1s^+$ and $2\Gamma_7^-$-to-$1s^+$ transitions which are strongly allowed for small sizes lose their oscillator strengths as the size increases due to the crossing of the levels discussed above. The EMA labels for the transitions shown in Table IV refer to the smallest size. We note that in CdSe QD's, the spin-orbit splitting for the first VB level is about 340 meV for a radius of 8.9 Å. This gradually increases, with the size of the QD, towards the bulk value of 440 meV. Further, as in CdS, some transitions such as $4\Gamma_8^-$ to $1\Gamma_6^+$ ($1D^-$ to $1s^+$ in the EMA), which would be expected to be forbidden from EMA, acquire oscillator strength at certain sizes due to mixing with nearby levels of the same symmetry, induced by the cubic perturbation.

The first even-parity splitoff level is of Γ_6^+ symmetry ($1p^+$ in the EMA) and is connected to the $1p^-$ CB level. For small sizes, this VB level lies above the first Γ_6^+ level arising from the $J=\frac{3}{2}$ band and corresponding to the $F=7/2^+$ EMA level. However, as the size increases, the Γ_6^+ level from the $J=\frac{3}{2}$ band has lower energy than the splitoff Γ_6^+ level due to reduced quantum confinement. This explains the loss in oscillator strength by the $1\Gamma_6^+$-to-$1p^-$ (i.e., $1\Gamma_6^+$-to-$1\Gamma_7^-$ and $1\Gamma_6^+$-to-$1\Gamma_8^-$) transitions, shown in the table, as the QD size increases. On the other hand, the transitions from the p-like VB to the p-like CB, viz., $1\Gamma_8^+$ to $1\Gamma_7^-$ and $1\Gamma_8^-$ and $2\Gamma_8^+$ to $1\Gamma_7^-$ and $1\Gamma_8^-$, remain strongly allowed for all sizes.

B. Optical-absorption spectra

We now compare the results of our calculations for CdSe and CdS QD's with experimental results available in the literature. In Fig. 3 we compare the size depen-

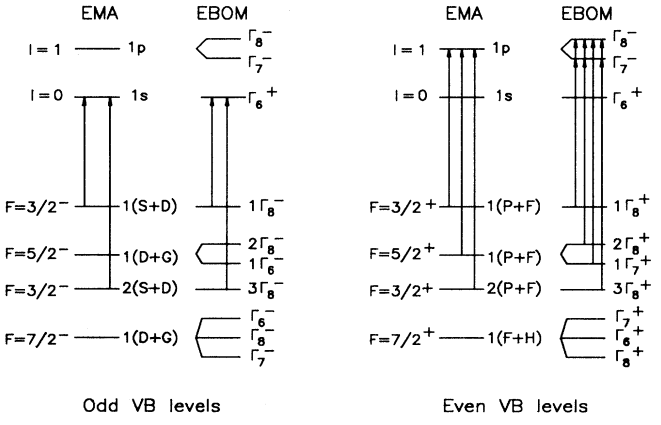

FIG. 2. Correspondence between the qualitative level structure of the near-band-edge energy levels obtained using the EBOM and the EMA, for CdSe. In the EMA, a four-band model for the $J=\frac{3}{2}$ VB and a single-band model for the conduction band (CB) have been used. The interband transitions, allowed according to the EMA selection rules, are also indicated. The splitoff band ($J=\frac{1}{2}$) levels are not shown.

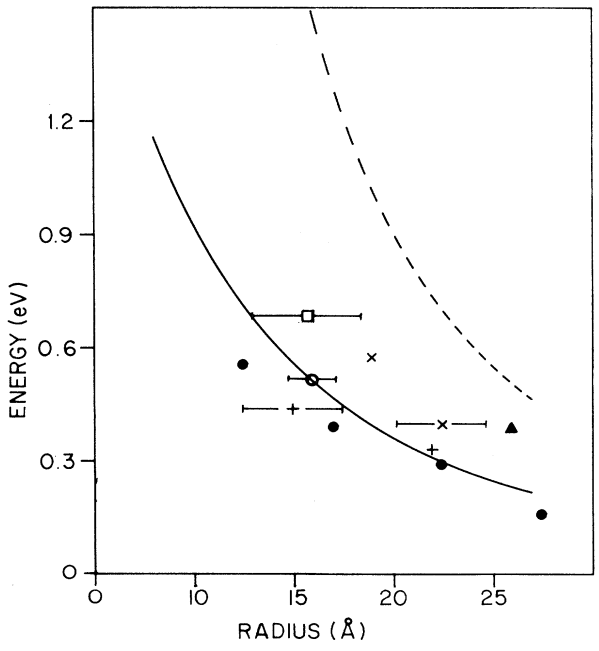

FIG. 3. The size dependence of the first interband transition in CdSe QD's calculated using the EBOM (solid line) and the single-band EMA (dashed line). The experimental data are also shown for comparison. These are taken from Refs. 3 (plus sign), 4 (open circle), 7 (cross), 11 (square), 13 (closed circle), and 14 (triangle).

dence of the experimental and theoretical values for the lowest transition frequency in CdSe QD's. The transition frequencies can be obtained from Table IV by including the Coulomb interaction between the electron and hole estimated in first-order perturbation theory using single-band EMA wave functions. This is given by[16] $E_{\text{coul}} = -1.786e^2/\epsilon R$, where ϵ is the dielectric constant of the material. The result of a single-band EMA calculation, with Coulomb interaction included, is also shown in the figure. All transition frequencies quoted are with respect to the bulk band gap, which for each experimental datum is taken at the appropriate temperature.

There is good agreement between the tight-binding theory and most of the experimental data. However, some of the experimental data are seen to be quite dispersed, with the absorption peak sometimes occurring at almost the same frequency even in nanocrystallites which differ in radius by as much as ~10 Å. This appears to indicate considerable uncertainty in the size of the crystallites in some samples. In all of these experimental data, the sizes have been quoted as measured, by transmission electron micrography or by small-angle x-ray scattering. However, it may be mentioned that quite frequently in the literature, the size of the QD's is quoted as having been estimated by applying the single-band EMA to the first absorption peak. As is apparent from Fig. 3, this could lead to a gross overestimation of the size, by 10 Å or more.

The absorption spectrum of a collection of QD's may be calculated as follows. The optical-absorption coefficient of a single quantum dot is given by

$$\alpha(\omega) \sim \sum_i \frac{f_i \Gamma_i}{(\omega - \Omega_i)^2 + \Gamma_i^2} , \tag{4}$$

where f_i is the oscillator strength, Ω_i the transition frequency, and Γ_i is the homogeneous half-width of the ith interband transition, and the sum is over all the transitions from the filled levels to the unfilled ones. For calculating the absorption spectrum of a collection of QD's with a distribution of sizes, we have to include the consequent inhomogeneous broadening, which may be taken into account by averaging Eq. (4) over a suitable size distribution. However, in the absence of a detailed knowledge of the size distribution, we assume simply that the Lorentzians in Eq. (4) may be replaced by δ functions, and that the size dispersion leads to a Gaussian dispersion of the transition frequencies. We assume also that the oscillator strengths are only weakly size dependent. Then, the total absorption coefficient for a dilute collection of quantum dots is given by

$$\alpha(\omega) \sim \sum_i f_i \exp[-(\omega - \bar{\Omega}_i)^2/\sigma_i^2] , \tag{5}$$

where $\bar{\Omega}_i$ are the transition frequencies appropriate to the average size, and σ_i is the net broadening of the ith transition.

It may be mentioned here that we have neglected the local-field correction, which arises from the fact that the electric-field penetration into a quantum dot depends on its dielectric function. This can cause a shift of the resonances and an exchange of oscillator strengths between them, leading to the modification of the absorption spectrum.[29] However, this modification would be qualitatively important only when the resonant contribution to the real part of ϵ dominates, i.e., near strong and sharp resonances. Using the observed homogeneous half-widths of 35–50 meV,[4,7,12] we estimate that for crystallites larger than about 10-Å radius, the local-field correction only leads to a more-or-less uniform reduction of all the near-band-edge transition strengths. However, in smaller QD's with reduced volume, the oscillator strength per unit volume will be large, and the local-field correction will have to be taken into account to correctly describe the features in the absorption spectrum.

In Fig. 4(a), CdSe QD's of radius 16 Å are considered, with the theoretical absorption spectrum compared with the experimental absorption spectrum of Bawendi *et al.*[4] In the calculated spectrum, a broadening proportional to the transition frequencies measured from the band edge has been used, with $\sigma_i = 0.2(\bar{\Omega}_i - E_g)$. As the oscillator strengths and transition frequencies have been calculated only for the sizes mentioned in Table IV, the data for $R = 16$ Å are obtained by linear interpolation. The experimental and theoretical spectra agree well in the relative strengths of the two resolved absorption peaks, and in the position of the first. However, the second peak in the calculated spectrum is about 150 meV below that in the experimental spectrum. The homogeneously broadened single-particle spectrum has also been investigated by Bawendi *et al.*[4] using the PLE technique. In

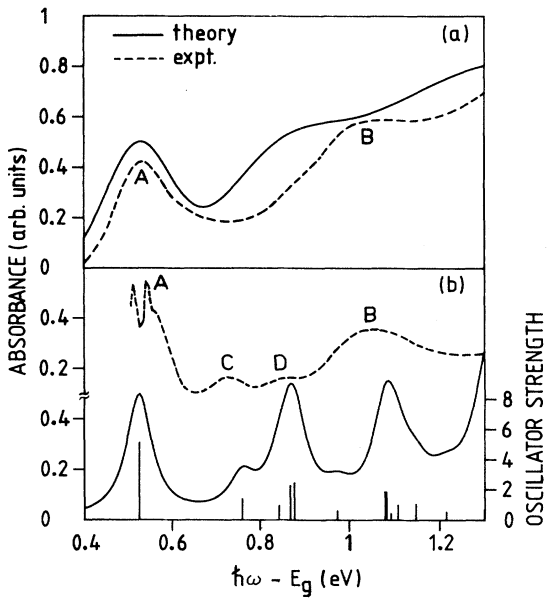

FIG. 4. (a) Calculated (solid line) and experimental (dashed line, adapted from Ref. 4) absorption spectra of a collection of CdSe QD's with mean radius 16 Å. (b) Theoretical single-particle absorption spectrum with homogeneous half-widths of 35 meV compared with the PLE spectrum taken from Ref. 4. The calculated individual transitions are indicated by vertical lines with heights proportional to the oscillator strengths.

Fig. 4(b), the PLE spectrum for 16-Å CdSe QD's is compared with our calculated homogeneously broadened absorption spectrum. We have used Lorentzian broadening with a half-width of 35 meV. The major individual transitions are also indicated, by straight lines, with the height of the line representing the strength of the transition. We shall denote the two peaks in the experimental absorption spectrum [Fig. 4(a)] by A and B. The PLE spectrum resolves further substructure, denoted by C and D, between peaks A and B. As is apparent from the theoretical plots, the first peak A is due mainly to a single transition, the $1\Gamma_8^-$-to-$1\Gamma_6^+$ transition, and may be denoted $1(S+D)^-$ to $1s^+$ in the spirit of the EMA. It is to be noted that as the transition frequencies given in Table IV include only the confinement energy, the Coulomb binding energy of 230 meV should be subtracted to obtain the net shift from the band gap shown in Figs. 4(a) and 4(b). The peak B is due to a large number of transitions, as can be seen from the figure. The calculated single-particle spectrum very well reproduces the frequencies of the peaks seen in the PLE spectrum. However, the two differ considerably in the relative height of the peak D, which is very much stronger in the calculated spectrum, though the strength of the B, C, and D peaks taken together compares well with the PLE. This difference is manifested in the absorption spectra also, as the 150-meV discrepancy mentioned earlier. This discrepancy may be due to the simple way in which the Coulomb interaction is included in the calculation, using the EMA value for the $1s$-$1s$ exciton for all the transitions, and the neglect of the surface polarization energy. A more elaborate calculation of these energies within tight-binding theory may lead to a better agreement.

It may be mentioned that the many closely spaced transitions that make up the peak B remain unresolved in the PLE spectrum of Ref. 4. Thus the width of the peak B in the PLE spectrum is not entirely due to the homogeneous broadening of a single transition, but is due to the presence of a number of closely spaced unresolved transitions as well. Further, in the hole-burning experiment of Bawendi *et al.*,[4] the peaks A, B, and C bleach together. This observation is consistent with our results, as some transitions with the $1s$ CB level in common contribute to each of these peaks.

Figure 5 gives the calculated absorption spectra for CdS QD's of radius 11 Å, as well as the experimental spectrum of Esch *et al.*[5] They estimated the size of their nanocrystallites by applying the single-band EMA with a finite confinement potential to the first absorption peak, and obtained a size of 13.4-Å radius. However, by matching their first peak to the tight-binding result, we estimate the size of their crystallites to be 11-Å radius. Our calculated spectrum for 11-Å crystallites is obtained by interpolation between the two sizes of 9 and 12 Å. Esch *et al.* obtain two resolved peaks in their absorption spectrum at 657 and 1168 meV above the bulk band gap. These may be compared with our calculated spectrum, with the corresponding two peaks occurring at 710 and 1190 meV above the bulk band gap. We have used a Gaussian broadening of 200 meV for the lowest two transitions and 225 meV for the rest. We note that a

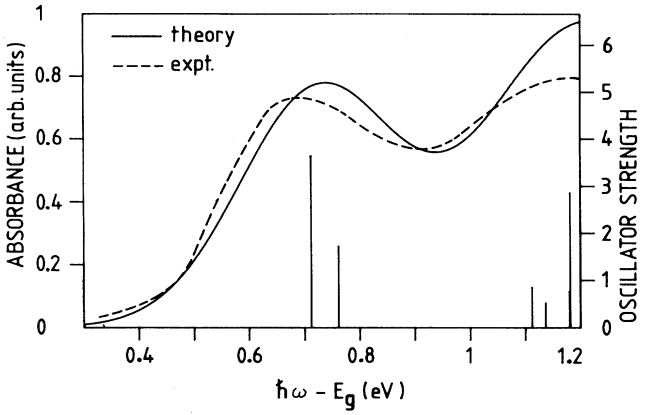

FIG. 5. Calculated (solid line) and experimental (dashed line, adapted from Ref. 5) absorption spectra of a collection of CdS QD's with mean radius 11 Å. The individual transitions in a single QD are indicated by vertical lines with heights proportional to the oscillator strengths.

Coulomb binding energy of 390 meV, appropriate for 11-Å CdS QD's, is to be subtracted from the confinement energies given in Table III to get the transition frequencies in the absorption spectrum. Quite unlike the case of CdSe, two transitions, viz., the $1\Gamma_8^-$-to-$1\Gamma_6^+$ and the $1\Gamma_7^-$-to-$1\Gamma_6^+$ transitions, separated by only 50 meV, make up the first observed peak. This difference between CdSe and CdS arises because of their very different spin-orbit splittings. This first peak may be denoted by $1(S+D)^-$ to $1s^+$. The second peak is made up mainly of the following transitions: the $1\Gamma_8^+$ to $1\Gamma_8^-$ and $1\Gamma_8^+$ to $1\Gamma_7^-$, which are almost degenerate, and the $1\Gamma_6^+$ to $1\Gamma_7^-$ and $1\Gamma_6^+$ to $1\Gamma_8^-$, which are also almost degenerate. The latter two are just outside the energy range shown in Fig. 5. In between are two weaker transitions, as can be seen from the lines representing the individual transitions.

The calculated optical-absorption spectra of CdSe and CdS QD's discussed above agree fairly well with the experimental results. The slight discrepancies that exist may be related to a number of factors, an important one being the sensitive size dependence of the energy levels in QD's. A 10% variation in size could result, on the average, in a 15% variation in the confinement energy, in the size range considered by us. Thus, an uncertainty of 1 Å in a 16-Å-radius QD could lead to a variation of $\sim$100 meV. There could be similar effects due to shape and surface structure uncertainties as well. Again, most experiments, including those of Ref. 4, have been performed on wurtzite QD's. However, the wurtzite structure can be considered as a weak perturbation on the zinc-blende structure, as the crystal-field splitting in both CdS and CdSe is small, and our calculation for the cubic form can be expected to provide a reasonably accurate description of the hexagonal form as well.

IV. CONCLUSIONS

We have presented a tight-binding calculation, using an effective-bond-orbital model, of the optical-absorption

spectra for cubic semiconductor quantum dots of spherical shape. We have developed a correspondence between the interband transitions given by tight-binding theory and those given by multiband EMA in the spherical approximation. This allows us to apply, to a large extent, the stringent EMA selection rules to describe the interband transitions, and to label these transitions, using the simpler EMA notation, in terms of the envelope-function angular momenta. For illustration, we have considered CdS and CdSe QD's, which are representative of materials with small and large spin-orbit splitting. By introducing a Gaussian inhomogeneous broadening, we have obtained optical-absorption spectra which are in good quantitative agreement with existing experiments on both CdS and CdSe. Our results show that the experimentally observed peaks in the absorption spectra correspond to a number of transitions which are not resolved partly because of the inhomogeneous broadening. It should be possible to resolve these broadened peaks in samples with smaller size distributions as well as by using hole-burning and photoluminescence excitation techniques. The PLE spectrum of 16-Å CdSe QD's reported in Ref. 4 resolves some of these transitions. The comparison of the PLE spectrum with our calculated single-particle absorption spectrum shows good agreement in the positions of the peaks, but indicates an intriguing difference in the distribution of oscillator strengths between two of the peaks. Finally, we note that the size of the QD could be grossly overestimated if it is obtained by comparing the experimental absorption edge with the single-band EMA calculation, as is sometimes reported in the literature.

ACKNOWLEDGMENTS

The authors are deeply indebted to Dr. K. C. Rustagi for many stimulating discussions and critical comments on the manuscript.

[1]A. I. Ekimov, Phys. Scr. **T39**, 217 (1991); G. W. Bryant, Comments Condens. Matter Phys. **14**, 277 (1989).
[2]L. E. Brus, Appl. Phys. A **53**, 465 (1991).
[3]N. F. Borrelli, D. W. Hall, H. J. Holland, and D. W. Smith, J. Appl. Phys. **61**, 5399 (1987).
[4]M. G. Bawendi, W. L. Wilson, L. Rothberg, P. J. Carroll, T. M. Jedju, M. L. Steigerwald, and L. E. Brus, Phys. Rev. Lett. **65**, 1623 (1990).
[5]V. Esch, K. Kang, B. Fluegel, Y. Z. Hu, G. Khitrova, H. M. Gibbs, S. W. Koch, N. Peyghambarian, L. C. Liu, and S. H. Risbud, Int. J. Nonlin. Opt. Phys. **1**, 25 (1991).
[6]M. L. Steigerwald, A. P. Alivisatos, J. M. Gibson, T. D. Harris, R. Kortan, A. J. Muller, A. M. Thayer, T. M. Duncan, D. C. Douglass, and L. E. Brus, J. Am. Chem. Soc. **110**, 3046 (1988).
[7]A. P. Alivisatos, A. L. Harris, N. J. Levinos, M. L. Steigerwald, and L. E. Brus, J. Chem. Phys. **89**, 4001 (1988).
[8]A. P. Alivisatos, T. D. Harris, L. E. Brus, and A. Jayaraman, J. Chem. Phys. **89**, 5979 (1988).
[9]V. L. Colvin, A. P. Alivisatos, and J. G. Tobin, Phys. Rev. Lett. **66**, 2786 (1991).
[10]Y. Wang and N. Herron, Phys. Rev. B **42**, 7253 (1990).
[11]U. Woggon, M. Müller, U. Lembke, I. Rückmann, and J. Cesnulevicius, Superlatt. Microstruct. **9**, 245 (1991).
[12]C. Splegelberg, F. Henneberger, and J. Puis, Superlatt. Microstruct. **9**, 487 (1991).
[13]N. Nogami, S. Suzuki, and K. Nagasaka, J. Non-Crystal. Solids **135**, 182 (1991).
[14]S. H. Park, R. A. Morgan, Y. Z. Hu, M. Lindberg, S. W. Koch, and N. Peyghambarian, J. Opt. Soc. Am. B **7**, 2097 (1990).
[15]K. I. Kang, B. P. McGinnis, Sandalphon, Y. Z. Hu, S. W. Koch, N. Peyghambarian, A. Mysyrowicz, L. C. Liu, and S. H. Risbud, Phys. Rev. B **45**, 3465 (1992).
[16]L. E. Brus, J. Chem. Phys. **80**, 4403 (1984).
[17]A. I. Ekimov, A. A. Onushchenko, A. G. Plyukhin, and Al. L. Éfros, Zh. Eksp. Teor. Fiz. **88**, 1490 (1985) [Sov. Phys.—JETP **61**, 891 (1985)].
[18]J. B. Xia, Phys. Rev. B **40**, 8500 (1989).
[19]S. V. Nair, in *Proceedings of the Solid State Physics Symposium, Indian Institute of Technology, Madras* (Department of Atomic Energy, India, 1989), Vol. 32C.
[20]P. C. Sercel and K. J. Vahala, Phys. Rev. B **42**, 3690 (1990).
[21]P. E. Lippens, and M. Lannoo, Phys. Rev. B **39**, 10 935 (1989); **41**, 6079 (1990).
[22]S. V. Nair, L. M. Ramaniah, and K. C. Rustagi, Phys. Rev. B **45**, 5969 (1992).
[23]S. V. Nair, L. M. Ramaniah, and K. C. Rustagi, Phys. Rev. Lett. **68**, 893 (1992).
[24]Y.-C. Chang, Phys. Rev. B **37**, 8215 (1988).
[25]J. C. Slater and G. F. Koster, Phys. Rev. **94**, 1498 (1954).
[26]G. T. Einevoll and Y.-C. Chang, Phys. Rev. B **40**, 9683 (1989).
[27]Y. R. Wang and C. B. Duke, Phys. Rev. B **37**, 6417 (1988).
[28]G. Bastard, *Wave Mechanics Applied to Semiconductor Heterostructures* (Les Editions de Physique, Paris, 1988).
[29]L. Genzel and T. P. Martin, Surf. Sci. **34**, 33 (1973).